

Spectral and Microscopic Properties of Calcium Silicate Hydrate Polymer Nanocomposites

L. Raki¹, S. C. Mojumdar², S. Lang³ and D. Wang⁴

¹*Institute for Research in Construction, National Research Council Canada,
Ottawa, Ontario, Canada*

²*University of Toronto, Faculty of Forestry,
Toronto, Ontario, Canada*

³*Steacie Institute for Molecular Sciences, National Research Council Canada,
Ottawa, Ontario, Canada*

⁴*Institute for Chemical Processes and Environmental Technology, National
Research Council Canada, Ottawa, Ontario, Canada*

Abstract

Calcium silicate hydrates (C-S-H), which form during the hydration of the silicate phases present in Portland cement, are the main binding phases that result in the formation of a hardened mass. The structure of C-S-H polymer nanocomposites formed as a result of a co-precipitation technique under fixed temperature and pH conditions was studied. XRD analysis and other related analytical techniques such as: ¹³C and ²⁹Si MAS-NMR, FTIR, TGA/DTA, TMA and TEM were used to characterize a selected number of C-S-H samples intercalated with polyvinyl alcohol (PVA) at different concentrations.

1. Introduction

Organic-inorganic hybrid materials, composed of a layered inorganic matrix with organic polyconjugated macromolecules in the interlayer space, have been the subject of the thorough attention of researchers for the past 5-15 years [1-3]. One of the very important materials of this type is the so called macro-defect-free (MDF) material at microscopic and nano-metric levels [4, 5]. Polymers are very important additives in the manufacture and processing of various materials, where the modification of interfaces and particle surface functionalizations are largely influenced by the model of the functional polymer.

In concrete technology, admixtures in the form of organic and inorganic polymers are widely used to modify its fresh and hardened properties. Therefore, it is of great importance to explore the mechanisms of interaction between these admixtures and cement hydrates, in order to obtain a better understanding of processes involved during the hydration of cement systems at the nanoscale. The nature and properties of C-S-H phases are central to the science of cement and concrete and their study could lead to successful prediction and control of the performance of concrete.

The reaction of Portland cement with water produces a number of products, the most important of which is called calcium silicate hydrate gel (C-S-H). C-S-H is the main binding phase in cement-based systems and is characteristically poorly crystalline or nearly amorphous in a young cement paste. C-S-H can be synthesised by reaction between Ca(OH)_2 and silicic acid, or between solutions of calcium/sodium silicates and a soluble calcium salt.

Advanced studies on C-S-H intercalation by polymers has opened up new routes to develop nanocomposites. The pioneering work of Matsuyama et al [1, 2] revealed the structural versatility of C-S-H composite products as a function of the degree of polymerization (Ca/Si ratio) and the nature of the organic polymers. The formation of C-S-H /polymer complexes was supported by results obtained by means of XRD, TGA, chemical analysis and MAS NMR. More recent work on the development of new C-S-H-based composites was carried out by Minet *et al.*[6, 7].

Physico-mechanical properties of different C-S-H specimens were reported in a study on compact samples of C-S-H powders using length change, microhardness and porosity measurements [8]. Their results showed a dependence of the intrinsic mechanical properties on the degree of polymerization (Ca/Si). A very innovative approach in the study of expansive behaviour of C-S-H compacts immersed in different salts solutions was extensively discussed [9] in the context of its significance in cement science. Interaction of C-S-H with organic intercalates was recently investigated [10]. It was concluded that the use of admixtures and different curing temperatures could have a significant effect on the nanostructural behaviour of C-S-H binders in concrete.

The main objective of this paper is to elucidate the structural properties of C-S-H/PVA materials obtained by assembly of C-S-H particles in the presence of PVA molecules, via a co-precipitation technique. A combination of complementary analytical techniques was used to relate chemical characteristics to physical properties of selected C-S-H/PVA composites.

2. Experimental

Materials and Synthesis

Commercial polyvinyl alcohol (Sigma Chemical Co., St. Louis, USA) was used in this study. The compounds used for the synthesis of C-S-H were $\text{Ca(NO}_3)_2 \cdot 4\text{H}_2\text{O}$ and NaOH (Fisher Scientific, Fair Lawn, New Jersey, USA), and $\text{Na}_2\text{SiO}_3 \cdot 9\text{H}_2\text{O}$ (National Silicates, Toronto Canada). C-S-H and its nanocomposites, C-S-H/PVA were prepared following the procedure described elsewhere [11].

Analytical Procedures

The powder X-ray diffraction (XRD) patterns were performed on a Scintag XDS 2000 X-ray diffractometer using Cu-K α radiation at 45 kV and 35 mA between 4 and 65 ° (2 θ) with a graphite secondary monochromator.

TEM samples were prepared by suspending the particles in acetone followed by sonication for several minutes. One drop of the particle/acetone suspension was placed onto a holey carbon grid and was dried in air. The dried grid was then loaded into a double tilt sample holder. The sample was thus examined with a Philips CM20 STEM equipped with a Gatan UltraScan 1000 CCD camera and an energy dispersive X-ray spectrometer: INCA Energy TEM 200. Both BF and HRTEM images were taken at 200 kV.

²⁹Si MAS NMR spectra were recorded at 39.7 MHz, on a TecMag Apollo spectrometer using a 7 mm Doty probe. Chemical shifts are reported relative to an external tetramethylsilane reference sample. Samples were spun in 7 mm zirconia rotors at 4 kHz, and a 7 microsecond 90-degree pulse was used on both spectrometers. ¹³C CPMAS and DDMAS (dephasing period of 40 μ s) NMR spectra were acquired on a Bruker Avance 200 spectrometer. Samples were packed in 7 mm zirconia rotors and spun at 4 kHz. Commercial MAS probes provided by Bruker and Chemmagetics were used.

FTIRPAS spectra were recorded by using a MTEC Model 200 photoacoustic detector. Thermal analyses on powder samples (~ 20 mg) were carried out using a simultaneous SDT Q600 T.A.I. instrument at 10 °C/min from room temperature (RT) to 1000 °C under nitrogen atmosphere using a flowing rate 100 ml/min.

Thermal analysis on powder samples (~20 mg) was carried out using a simultaneous SDT Q600 T.A.I. instrument at 10 °C/min from room temperature (rT) to 1000 °C under nitrogen atmosphere using a flowing rate 100 mL/min.

For thermal conductivity measurements, a Mathis TC-01 system, which uses the modified hot wire technology, was used. Samples were tested as they were synthesized and purified without additional sample preparation. During all measurements, a 652 g weight was placed on the top of the sample to ensure a good contact between the sample and sensor. The test times utilized were 2.3-5.0 seconds.

TMA measurements were carried out using a model 2940 TMA instrument, a product of TA Instruments Inc. The instrument was calibrated according to the TMA instrument calibration procedure from the instrument manual. A four step calibration was performed: the probe calibration, the force calibration, the cell constant calibration with the aluminium calibration standard, and the temperature calibration with the indium calibration standard. The following test conditions were used for the calibration and for the sample testing: heating rate: 1 °C/min,

temperature range: 5 to -20°C (cooling/heating cycle), force: 0.05N, probe type: expansion (~2 mm diameter). The disc type samples were placed between the quartz platform and probe. Liquid nitrogen was used for cooling to reach the lower than room temperature. Data was analysed using the Universal Analysis 2000 software (version 4.1 d) from TA instruments.

3. Results and Discussion

XRD analysis has been presented by the authors in previous studies [11]. Patterns of different samples of C-S-H with increased concentrations of PVA exhibited some differences compared to the .XRD profile of pure C-S-H. The presence of peaks having characteristics of C-S-H at ca. 0.306, 0.28 and 0.182 nm as well as the basal plane (002) reflection above 10° 2θ (>1.0nm) were evident. The peaks become broader with increasing PVA concentration as a result of a turbostratic disorder (displacement of silica sheets in the (a,b) plane) , but only the (002) reflection shows a peak shift as its position is a function of the interlayer distance between the “dreierketten” chains [12].

Thermal analysis of PVA, C-S-H and C-S-H/PVA samples is summarized in Table 1. Significant differences in the thermal decomposition properties of C-S-H, PVA and C-S-H/PVA samples were observed. From RT to 250 °C: C-S-H decomposition [10] occurs due to loss of molecular water with DTA peaks at 71–134 °C. In the case of C-S-H/PVA material, the decomposition temperature (T_d) in this region is variable depending on the synthesis and material compositions. Within the 250-550 °C range, decomposition of the polymeric material is observed [10]. DTA curves for C-S-H/PVA material as well as PVA exhibit DTA peaks in the temperature range 283-459 °C. The shift of the DTA peak to the higher temperature in C-S-H/PVA material compared to pure PVA and C-S-H is due to the confinement of the organic moieties inside C-S-H layers. Beyond 550 °C, the decomposition is a result of both structural water and CaCO₃ [13].

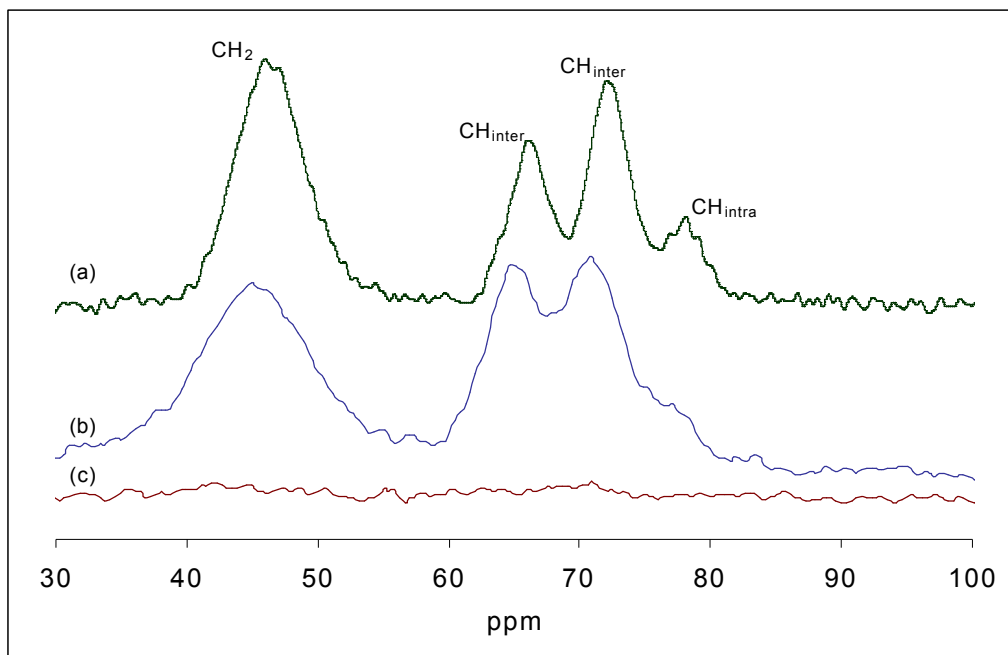
Table 1

Material	T_d / °C	DTA peak / °C
C-S-H	250, over 550	71, 693
C-S-H/PVA	250, 550, over 550	134, 356, 701
PVA	250, 370, 500	57, 283, 459

The ¹³C CPNMR spectra of C-S-HPVA material (Figure 1) have been compared to pure commercial PVA spectra. The spectra of pure PVA (Fig.1 a) has been analysed based on a previous NMR investigation [14]. An NMR signal at about 45 ppm corresponds to the -CH₂- carbon and the signals at about 65-77 ppm are due to the -CH- carbon. The splitting of the -CH- carbon signal into three peaks was assigned following the nature of hydrogen bonding these -CH-

groups are involved in. The peak at 77 ppm represents a $-\text{CH}-$ group with two intramolecular hydrogen bonds, while the peak at about 71 ppm is due to a $-\text{CH}-$ with one intermolecular hydrogen bond and the peak at 65 ppm is assigned to a $-\text{CH}-$ group with no hydrogen bond. The ^{13}C CPNMR spectra of C-S-H/PVA material (Fig 1b) shows a broad peak for the methylene signal at 44 ppm and only two methine carbon resonances shifted slightly to 70 ppm and 64. ppm. A shoulder replaced the peak originally located at 77 ppm. These observations imply that the intramolecular hydrogen bonds responsible for the agglomeration of PVA molecules are less present. Confinement of PVA molecules within the interlamellar space of C-S-H would be the most plausible explanation of such a behaviour.

Upon dipolar dephasing (DD) conditions [15]], the methylenic and methinic ^{13}C signals completely disappear. The absence of $^{-13}\text{CH}_2-$ and $^{-13}\text{CH}-$ peaks is indicative of the rigidity of the methylenic and methinic chains, in good agreement with an all trans conformation of the carbon backbone of PVA. On the basis of the XRD results, such a conformation was also confirmed and justified by a



single linear extension conformation of PVA molecules.

Figure 1: ^{13}C CP-MAS NMR of (a) PVA, (b) C-S-H/PVA, and (c) CP/DD MAS of C-S-H/PVA

In the case of ^{29}Si , the analysis is based on the Q^n classification [16] where Q represents a SiO_4^{4-} unit and the degree of connectivity, n, is related to the oxygen

bond number between the SiO_4^{4-} units. The ^{29}Si MAS NMR spectra of the C-S-H/PVA material is presented in Figure 2. According to the ^{29}Si MAS NMR spectra, characteristic Q^1 and Q^2 sites in the silicate chains are observed in all case, which is comparable to tobermorite. The ^{29}Si MAS NMR spectra of C-S-H and C-S-H/PVA material contain mainly the Q^2 peak. However, a weak Q^1 peak or a shoulder is present in all spectra at about -95 ppm. The broadening of the Q^2 peaks at ^{29}Si MAS NMR spectra, of C-S-H/PVA material is due to the structural deformation, caused by the intercalation of PVA molecules into C-S-H. The addition of PVA decreased the Q^n intensity, indicating a “virtual” lengthening of the silicate chains as a result of PVA molecules presence in the interlamellar space of C-S-H.

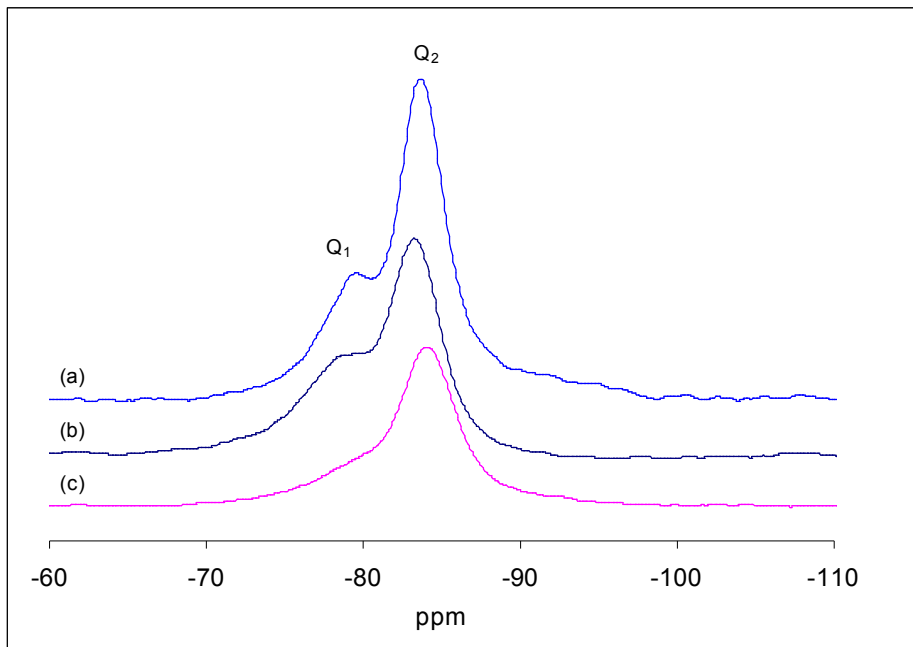


Figure 2. ^{29}Si CP-MAS NMR of (a) C-S-H, (b) C-S-H/PVA (0.7-0.05) and (c) C-S-H/PVA (0.7-0.5)

All FTIR spectra of C-S-H, PVA, and related C-S-H/PVA materials contain a characteristic set of bands in the range $973\text{--}978\text{ cm}^{-1}$ (Table 2). These are the most intensive bands in all spectra and can be assigned to Si-O stretching vibration of the Q^2 tetrahedra. The weak bands in the range $811\text{--}841\text{ cm}^{-1}$ are present in C-S-H and C-S-H/PVA samples, and are assigned to Si-O stretching vibrations of the Q^1 tetrahedra. The Si-O-Si bands are present at $669\text{--}671\text{ cm}^{-1}$. The bands at $3740\text{--}3742\text{ cm}^{-1}$ are due to Si-OH stretching in the isolated Si-OH species. These are the key information of the structure of C-S-H and C-S-H/PVA

materials. The stretching bands at 3390–3445 cm^{-1} can be attributed to water molecules. This observation is consistent with the observed decrease in water content with increasing polymer contents for these samples. At higher polymer contents, less H_2O molecules can be accommodated within the layer. The bands in the range of 1593–1645 cm^{-1} are due to H-O-H bending vibrations of H_2O molecules. Other bands at 448–453 cm^{-1} are due to the internal deformation of SiO_4 tetrahedra. The bands at 1385-1426 cm^{-1} correspond to the asymmetric stretching (ν_3) of CO_3^{2-} (It is not possible to prevent incorporation of CO_2 during sample preparation)

The characteristic vibration bands of PVA and C-S-H/PVA materials are shown at 3390 – 3441 cm^{-1} (-OH), 2933 – 2941 cm^{-1} (- CH_3), 2858 – 2859 cm^{-1} (- CH_2), 1430 – 1438 cm^{-1} (O=C-OR), 1016 – 1095 cm^{-1} (C-O-C) and 879 – 899 cm^{-1} (-CH). The shifted presence of PVA bands in C-S-H/PVA materials is indicative of PVA molecules intercalation between C-S-H sheets, as it is also supported by the XRD and SEM results [10].

Table2. FTIR spectral bands (4000-400 cm^{-1}) of PVA, C-S-H and C-S-H/PVA materials

Assignments	C-S-H	C-S-H-PVA (0.7-0.05)	C-S-H-PVA (0.7-0.15)	C-S-H-PVA (0.7-0.30)	C-S-H-PVA (0.7-0.5)	C-S-H-PVA (0.7-0.75)	PVA
Si-O	973, 821	981, 840	976, 841	973, 842	974, 842	974, 842	-
Si-O-Si	670	669	669	669	669	668	-
Si-OH	3742	3741	3741	3441	3741	3742	-
H-O-H	1645	1640	1645	1646	1646	1645	-
OH	3390	3441	3441	3431	3421	3429	-
CH_3	-	2944	2933	2939	2941	2941	2941
CH_2	-	2854	2859	2860	2861	2858	2858
O=C-OR	-	1444	1430	1453	1452	1450	1438
C-O-C	-	1026	1016	1028	1021	1025	1095
CH	-	878	879	881	883	875	899
CO_3^{2-}	1385	1385	1385	1385	1385	1385	-
Others	448	453	451	451	449	449	-

The modified hot wire transient technique was applied to measure the thermal conductivity of the studied samples. This technique can non-destructively and accurately measure the thermal conductivity and thermal diffusivity of a material in seconds. The modification compared to the hot wire technique is that the heating elements are supported on a backing, which provides mechanical support, electrical insulation, and thermal insulation. Such modification eliminates the intrusive nature of the hot wire technique, thereby allowing solids to be tested without melting or otherwise modifying the sample to conform to the geometry of the test cell.

The measured thermal conductivities of PVA, C-S-H and C-S-H/PVA material samples at 25 and 50 °C are presented in Table 3. The following conclusions can be drawn from the thermal conductivity measurements.

1. An accuracy of 0.5 % or better was observed in the thermal conductivity measurements of each sample, indicating the high reliability of the measurements performed in the study.
2. An RSD value of 1.5 % or better was observed in each set of the measurements, illustrating the high reproducibility of the measurements conducted
3. The lowest thermal conductivity at 25 °C was observed for C-S-H; however, PVA exhibited the lowest thermal conductivity at 50 °C. C-S-HPN material exhibited the highest thermal conductivity in both cases. However, the highest thermal conductivity increase was observed for C-S-H. The thermal conductivity increases from 25 to 50 °C are 7.03, 17.46 and 14.85 % for PVA, C-S-H and C-S-H/PVA materials, respectively.

Improvement of PVA conductivity when reacted with C-S-H implies a better arrangement of individual molecules. This could only be justified by a dense confinement of these organic moieties, which was provided by the interlamellar space inside the C-S-H structure.

The TMA is based on measurements of the deformation of the specimen under low load during the temperature increase. Analysis of TMA curves leads to determination of transition temperature, degree of crystallinity and different of regions differing by thermal expansion. The dimension change and the coefficient of thermal expansion (α) are two very important parameters that can be determined by TMA. The dimension changes and coefficient of thermal expansion of PVA, C-S-H and C-S-H/PVA materials during heating and cooling are presented in Figs. 3 and 4, respectively. It is evident that the coefficient of thermal expansion of C-S-H/PVA materials is lower than that of C-S-H and PVA in both cases during heating and cooling. It proved that the C-S-H/PVA samples are more resistant to temperature change compared to C-S-H and PVA.

Table 3

Sample	Measured k^* / $\text{Wm}^{-1} \text{K}^{-1}$		Average of the Measured k / $\text{Wm}^{-1} \text{K}^{-1}$		Increase from 25 TO 50 °C / %	RSD / %	
	25 °C	50 °C	25 °C	50 °C		25 °C	50 °C
PVA	0.1068 0.1069 0.1046 0.1067 0.1062 0.1065	0.1139 0.1136	0.1063	0.11375	7.03	0.81	0.13
C-S-HPN material	0.1644 0.1647 0.1656 0.1660 0.1646 0.1647	0.1897 0.1893	0.1650	0.1895	14.85	0.39	0.11
C-S-H	0.09822 0.09812 0.10730 0.10720 0.09825 0.09827	0.1191 0.1187	0.1012	0.1189	17.46	4.61	0.17

*k: thermal conductivity

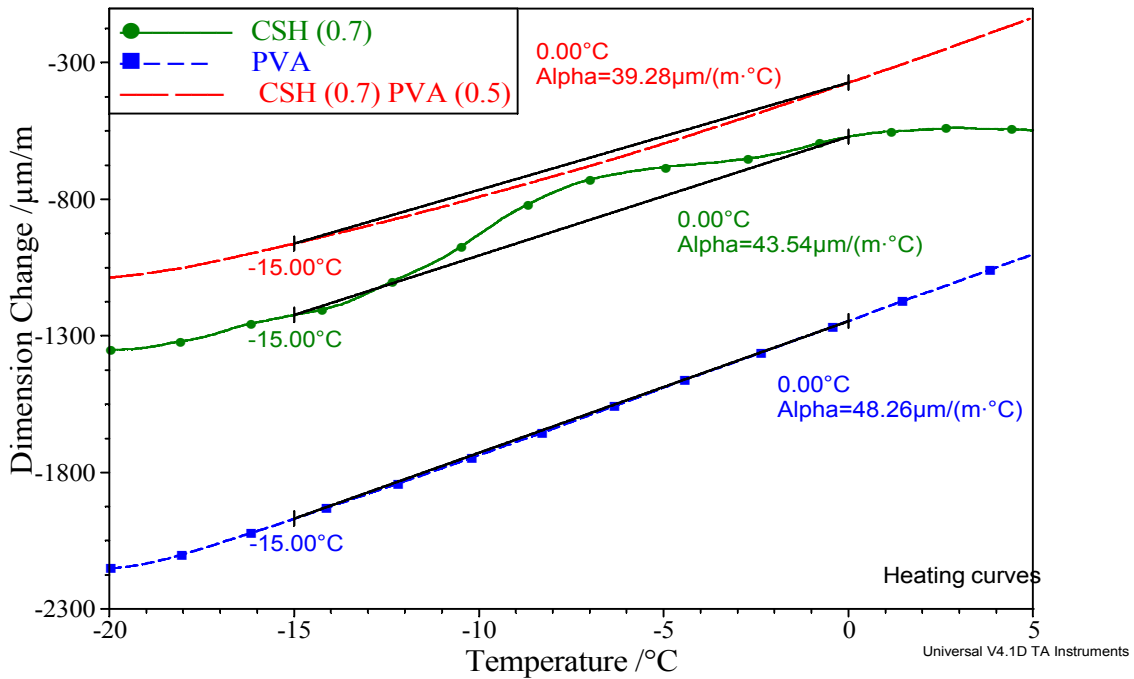


Figure 3. TMA (heating) curves of C-S-H, PVA and C-S-H/PVA sample

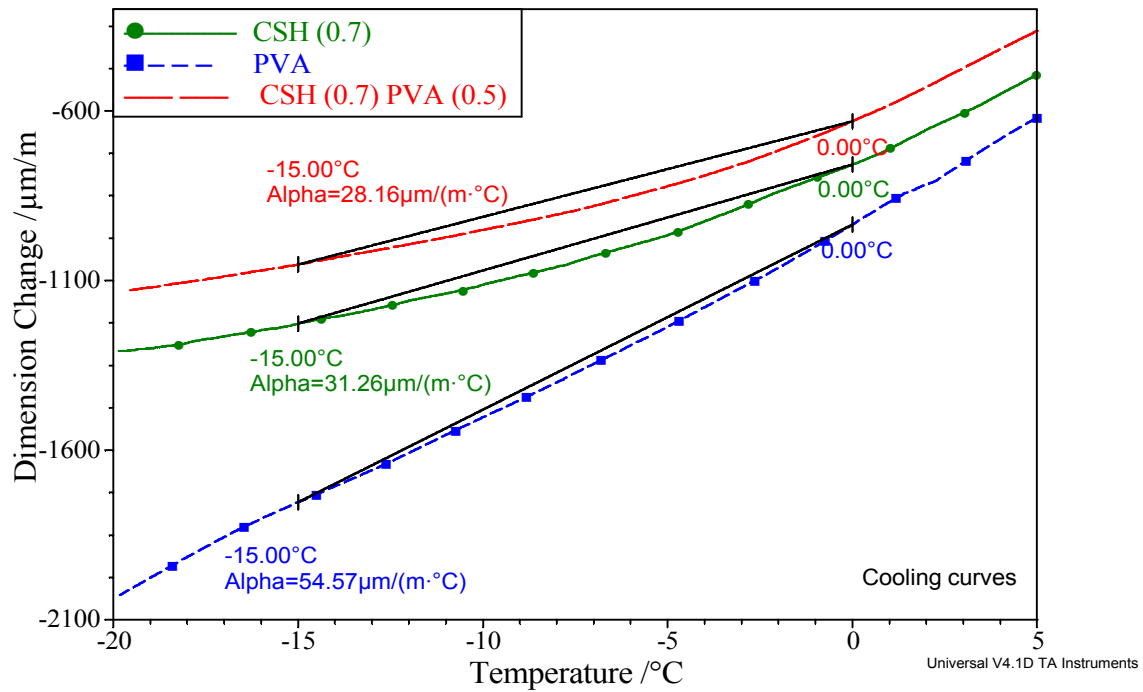
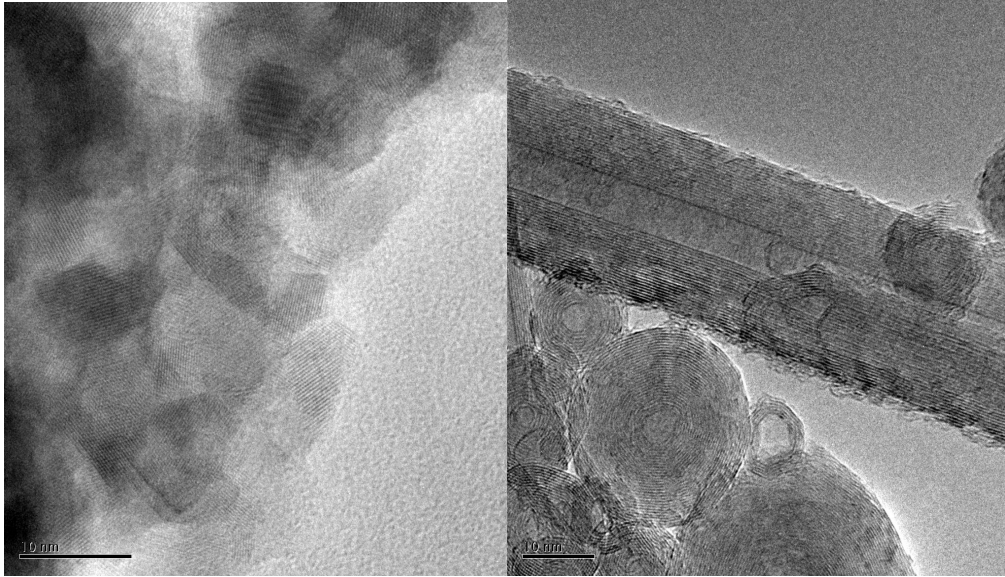


Figure 4. TMA (cooling) curves of C-S-H, PVA and C-S-H/PVA sample

Typical TEM images of synthetic C-S-H and C-S-H/PVA samples are shown in Figure 5. Significant differences in the nanostructure between both samples can be observed. Figure 5a represents a classical C-S-H structure as observed in numerous previous studies [17, 18]. Upon precipitation of C-S-H in the presence of PVA, the resulting structure undergoes major changes as shown in Figure 5b. The inorganic sheets of C-S-H while keeping their layered character have two different morphologies: tubular and “fingerprints” as is in the case for calcium aluminate polymer composites [19]. Analysis of C-S-H/PVA samples by FEG-SEM/EDS [11] confirmed the presence of PVA molecules in the interface polymer-C-S-H nanoparticles .



(a) (b)
Figure 5. TEM images for (a) C-S-H 0.7 and (b) C-S-H/PVA

4. Conclusions

New C-S-H-based polymer nanocomposites have been prepared via “Chimie douce” techniques and characterized by means of different analytical tools. The results showed an expansion of the interlamellar space of C-S-H upon intercalation of PVA molecules. These findings open up a new area of research in the field of cement science, where durability problems could be addressed and investigated at the nano scale.

Further investigative work to understand the interaction between PVA molecules and C-S-H at different Ca/Si ratio is in progress. A comprehensive study to elucidate the effect of these properties on the engineering characteristics of the resulting materials will be addressed through the use of XPS, DMA, and micro-hardness analysis.

Acknowledgment

The authors would like to thank Ms. A. Delgado for helping with FTIRPAS spectroscopic measurements. The authors would like to gratefully acknowledge the Natural Sciences and Engineering Research Council Canada (NSERC) for visiting fellowship grant to Dr.S. C Mojumdar.

References

1. H. Matsuyama and J.F. Young, *J. Mater. Res.*, 4 (1999) 16.
2. H. Matsuyama and J.F. Young, *Chem. Mater.* 11 (1999) 3389
3. E. P. Giannelis, *pp.Organometal. Chem*, 12 (1998).675.
4. Odler, *Special Inorganic Cement*, Chapter 13.3, "MDF cement", E & F. N. Spon (London, New York) 2000.
5. O. O. Popoola, W. M. Kriven, and J. F. Young, *J. Am. Ceram. Soc.*, 74 (8) (1991), 1928.
6. J. Minet, S. Abranmson, B. Bresson, A. Franceshini, H. Van Damme, and N. Lequeux, *J. Mater. Chem*, 16 (2006) 1379
7. J. Minet, S. Abranmson, B. Bresson, C. Sanchez, V. Montouillout, and N. Lequeux, *Chem. Mater*, 16 (2004) 3955.
8. J. J. Beaudoin, and R. F. Feldman, R. F., *Proceedings of the 8th International Congress on the Chemistry of Cement*, Rio de Janeiro, Brazil, (1986)
9. H. Dramé. J. J. Beaudoin. and L. Raki, accepted for publication. *Journal of Materials Science.*, 2007
10. J. J. Beaudoin, H. Dramé and L. Raki, L., submitted to *Journal of Materials Science*, 2007
11. S. C. Mojumdar and L. Raki, *J. Therm. Anal. Cal.*, 82 (2005) 89
12. R. F. Feldman and P. J. Sereda., *Engineering Journal*,(1970) 53.
13. H. F. W. Taylor. 1998. *Cement Chemistry*, 2nd Edn. Thomas Telford Publ., London. U.K.
14. M. Kobayashi, I. Ando, T. Ishii and S. Amiya, *J. Mol. Struc.*, 440 (1998) 155.
15. L. B. Alemany, D. M. Grant, T. D. Alger, R. and J. Pugmire, *J. Am. Chem. Soc*, 105 (1983) 6697
16. Z. H. Zanni, R. Rassem-Bertolo, S. Masse, L. Fernandez, P. Nieto and B. Bresson, *Magnet. Resonan. Imag.*, 14 (1996) 827.
17. I. Richardson, *Cem. Con. Res*, 34 (2004) 1733
18. X. Zhang, *J. Am. Ceram. Soc*, 83 (2000) 2600
19. O. O. Popoola, W. M. Kriven, and F. Young, *J. Am. Ceram. Soc*, 74 (1991) 1928.